AIP | Applied Physics Letters

# Work function engineering of single layer graphene by irradiation-induced defects

Jong-Hun Kim, Jin Heui Hwang, Joonki Suh, Sefaattin Tongay, Sangku Kwon, C. C. Hwang, Junqiao Wu, and Jeong Young Park

Citation: Applied Physics Letters **103**, 171604 (2013); doi: 10.1063/1.4826642
View online: http://dx.doi.org/10.1063/1.4826642
View Table of Contents: http://scitation.aip.org/content/aip/journal/apl/103/17?ver=pdfcov
Published by the AIP Publishing



# Work function engineering of single layer graphene by irradiation-induced defects

Jong-Hun Kim,[1] Jin Heui Hwang,[1] Joonki Suh,[2] Sefaattin Tongay,[2] Sangku Kwon,[1] C. C. Hwang,[3] Junqiao Wu,[2,4] and Jeong Young Park[1,a)]

[1]*Center for Nanomaterials and Chemical Reactions, Institute for Basic Science, and Graduate School of EEWS, KAIST, 373-1 Guseong Dong, Daejeon 305-701, South Korea*
[2]*Department of Materials Science and Engineering, University of California, Berkeley, Berkeley, California 94720, USA*
[3]*Beamline Research Division, Pohang Accelerator Laboratory (PAL), Pohang University of Science and Technology (POSTECH), Pohang 790-784, South Korea*
[4]*Division of Materials Sciences, Lawrence Berkeley National Laboratory, Berkeley, California 94720, USA*

(Received 31 July 2013; accepted 10 October 2013; published online 24 October 2013)

We report the tuning of electrical properties of single layer graphene by α-beam irradiation. As the defect density increases upon irradiation, the surface potential of the graphene changes, as determined by Kelvin probe force microscopy and Raman spectroscopy studies. X-ray photoelectron spectroscopy studies indicate that the formation of C/O bonding is promoted as the dose of irradiation increases when at atmospheric conditions. Our results show that the surface potential of the graphene can be engineered by introducing atomic-scale defects via irradiation with high-energy particles. © *2013 AIP Publishing LLC*. [http://dx.doi.org/10.1063/1.4826642]

Graphene is a two-dimensional carbon system with various novel properties, such as a zero-gap semi-metallic band, ballistic transport at submicron length scales, massless Dirac fermions, and an abnormal quantum Hall effect.[1,2] From a practical perspective, the extraordinarily high mobility[2] and thermal conductivity[3] have attracted much attention and made graphene one of the most interesting and promising materials in nanotechnology. Recently, large-area graphene was successfully synthesized via vacuum graphitization of SiC or chemical vapor deposition (CVD) using a Cu or Ni substrate.[4–6] Graphene grown by CVD can be transferred to a target substrate using poly-methylmethacrylate (PDMA) or poly-dimethylsiloxine (PDMS). However, there are still concerns about the possible formation of defects on the graphene surface which mainly result from: (i) the synthesis process, which is subject to the substrate state; or (ii) the transfer process, where the surface is exposed to various chemicals, electron microscopy, or the ionic fabrication process. It is, therefore, desirable to characterize and understand how defects affect graphene.[7–9] On the other hand, controlling defects is a promising approach for future applications since it can engineer, or modify, the intrinsic properties of graphene.[10] For example, field-effect transistors based on graphene need maneuverable p- and n-type conduction in the graphene to construct complex logic devices. As a transparent electrode, better electrical coupling (i.e., work function) between the graphene and the semiconductor, or enhanced electrical conductivity of the graphene is needed.[11,12] By using chemical treatment, graphene oxide or fluorinated graphene has been developed to have an open band gap.[13,14]

Beam irradiation is another attractive method to generate atomic-scale defects which tend to be more stabilizing as dopants.[15,16] Motivated by these requirements for possible applications, we studied how atomic-scale defects affect the properties of graphene in terms of chemical doping. In this work, we irradiated an α-beam ($He^{2+}$) on CVD-grown graphene to generate controlled defects. Raman spectroscopy and Kelvin probe force microscopy (KPFM) results show that such defects have the ability to modulate the doping level of graphene, which results in a shift in the Fermi-level, $E_F$.

The graphene was grown on a Cu substrate using the inductively coupled plasma CVD method.[17,18] Three pristine samples were irradiated with a 3.04 MeV $He^{2+}$ beam at doses of $1 \times 10^{14}$, $5 \times 10^{14}$, and $1 \times 10^{15}$ $cm^{-2}$. As-received pristine graphene was included as a reference for the following measurements. According to model calculations, formation of non-hexagonal rings or vacancies can take place under our irradiation conditions.[19] Raman spectra were measured at ambient conditions using a LabRAM HR UV-VIS-NIR Raman microscope (Horiba Jobin Yvon). The spot size was ~1 $\mu m^2$ and the power was kept at 0.5 mW to avoid local heating of the samples. $Ar^+$ ions with an excitation energy of 2.41 eV ($\lambda_D = 514.5$ nm) were used as the laser source. To characterize the beam-induced effects with respect to the surface potential, we conducted KPFM using an Agilent 5500 atomic force microscope. Pt/Ir-coated conductive cantilevers were used for non-contact mode and the topography and surface potential signal were measured simultaneously with a mechanical drive frequency of 75 kHz and AC modulation of 1 V at 20 kHz. By controlling the sample bias to nullify the capacitive force caused by the contact potential difference (CPD) between the tip and the sample, the local distribution of the surface potential can be mapped out. A synchrotron radiation source (4A2 and 10D beamlines of Pohang Accelerator Laboratory) was utilized for photoemission spectroscopy (PES) analysis. Photon energies of 650 eV and 72.5 eV were used for the core level and valence band, respectively.

a)Author to whom correspondence should be addressed. Electronic mail: jeongypark@kaist.ac.kr

 

Fig. 1(a) shows Raman spectra of the graphene samples after α-beam irradiation. Generally, Raman spectra of graphene feature two representative Lorentzian peaks: the G band at ~1600 $cm^{-1}$ and 2D band at ~2700 $cm^{-1}$. The former originates from the degeneracy of the longitudinal optic and in-plane transverse phonon modes ($E_{2g}$ symmetry) at the Brillouin zone center and the latter is due to the second-order Raman scattering process that involves two in-plane optic phonons near the K point. The intensity ratio of the D to G band, $I_D/I_G$, which commonly serves as a convenient way to assess defects or disordering, is negligible (~0.02) for pristine graphene while the ratio increases up to ~0.2 as the $He^{2+}$ dose increases, as shown in Fig. 1(b). The fact that the intensity ratio of 2D to G ($I_{2D}/I_G$) for the as-received graphene is close to ~0.4, with an ignorable D band at ~1350 $cm^{-1}$, verifies that the pristine graphene comprised one or two layers at most. Under the assumption that the defect density is sufficiently low such that the G band scattering is proportional to the number of point defects, the average distance between the generated defects, $L_D$, can be estimated using the empirical formula,[20,21] $L_D^2(\mathrm{nm}^2) = (1.8 \pm 0.5) \times 10^{-9} \lambda_D^4 \left(\frac{I_D}{I_G}\right)^{-1}$, so as to give $L_D$ of 40 ± 11 nm, 26 ± 7 nm, and 23 ± 7 nm for the samples irradiated with doses of $1 \times 10^{14}$, $5 \times 10^{14}$, and $1 \times 10^{15}$ $cm^{-2}$, respectively.

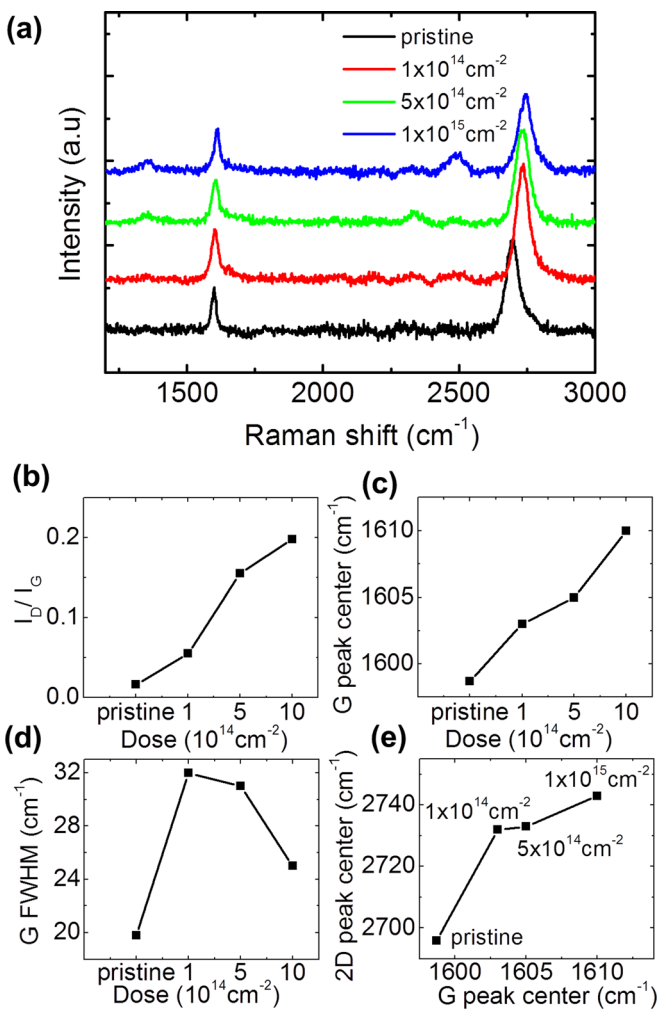


FIG. 1. (a) Raman spectra of pristine graphene and α-beam irradiated graphene samples. (b) D/G peak, (c) G peak position, (d) width of the G peak, and (e) G vs 2D peak position are plotted for pristine and irradiated graphene samples.

Figs. 1(c) and 1(e) show that α-beam irradiation resulted in a blue shift of the G peak. As reported in the literature,[22,23] either p- or n-doping results in an upshift of the G band, removing a Kohn anomaly in the $E_{2g}$ mode near the Γ point. Lorentzian fitting of the G bands provides information regarding structural disordering via full width at half maximum (FWHM), indicating doping-related variations (Fig. 1(d)). At first, the α-beam treatment increases the FWHM in the pristine graphene from 20.1 $cm^{-1}$ to 26.1 $cm^{-1}$ in the sample with the $1 \times 10^{14}$ $cm^{-2}$ dose. This can be attributed to the increased density of defects relaxing at the $\Gamma = 0$ condition. However, in the higher $He^{2+}$ fluence regime, the dopant-altered Fermi-level shift limits the available phonon decay such that the FWHM becomes narrow.[23] Therefore, Figs. 1(c) and 1(d) consistently imply that the irradiation treatment provides the doping effect. Determination of the doping polarity can be made by correlating the peak positions of the G and 2D bands because, unlike the upshift in the G peak, the 2D peak shifts upward with hole doping and downward with electron doping,[24,25] which modifies the phonon dispersion close to the Kohn anomaly, but also alters the equilibrium lattice parameter with the blue/red shift of the phonons. However, since the 2D phonons are too far apart from the Kohn anomalies at the K point, the first possibility is ignorable and variation of the 2D peak can be largely attributed to the doped charges: the blue shift for hole doping and the red shift for electron doping. Since both G and 2D peaks show blue shift, we conclude that irradiation-induced defects result in p-doping (i.e., the work function increases with irradiation).

A series of $570 \times 570$ $nm^2$ KPFM images of the graphene samples are shown in Fig. 2. All of the CPD maps are rescaled to the same intensity scale to clarify the dose-dependent variation where the brighter signal indicates a higher CPD. As shown in Fig. 2, the samples irradiated with a higher dose show brighter signals in the CPD maps. Fig. 3(a) shows histograms of the CPD distribution maps of the four specimens and each peak position was decided by Gaussian fitting in Fig. 3(b). As shown in Figs. 3(a) and 3(b), the upshift of the peak positions clearly shows that the CPD increases logarithmically with increasing dose from ~−150 mV to ~220 mV. Since the CPD is generally interpreted as the difference in work function between the tip and the sample surface, once the work function of the tip is determined, the work function of graphene, $W_{F,g}$, can be estimated as $\mathrm{CPD} = W_{F,g} - W_{F,tip}$ (see the inset in Fig. 3(b)). Before measuring the graphene system, the work function of the tip was calibrated by taking the CPD on the Cu foil. The measured CPD value is almost zero so that the tip work function is close to the work function of Cu (~4.7 eV)[26] within the error of measurement. Therefore, the subsequent KPFM results on the irradiated graphene revealed the variation of work function from 4.5 eV (pristine) to 4.9 eV. The work function of the pristine sample of ~4.5 eV is a reasonable value, compared with previously reported values.[27,28]

The histogram of the FWHM that was initially measured as 56 mV in the pristine graphene, increases to 96 mV in the graphene irradiated at $1 \times 10^{14}$ $cm^{-2}$, and then saturates at

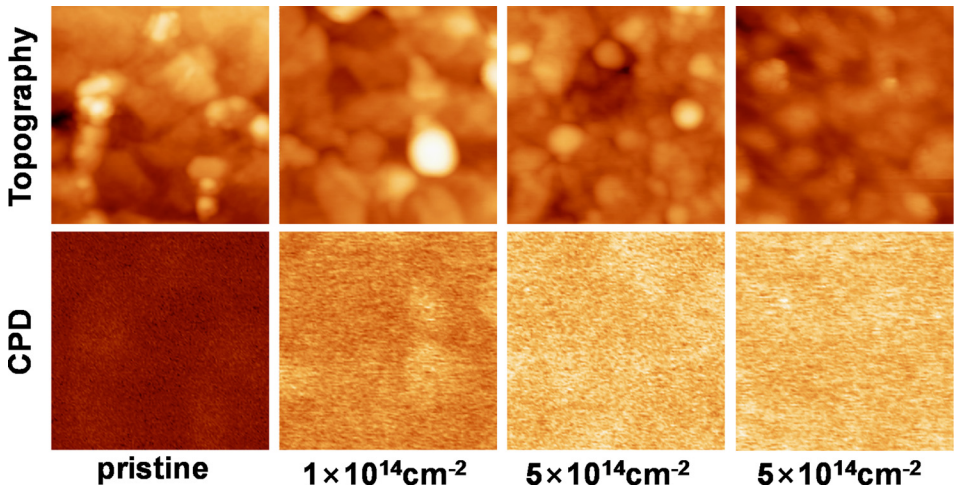


FIG. 2. Contact potential maps (bottom) and corresponding topography images (top) obtained using KPFM. The scan size is $570 \times 570\ nm^2$ and the contrast for all of the surface potential images was adjusted to an identical scale.

$\sim$104 mV in both graphene samples exposed to $5 \times 10^{14}\,cm^{-2}$ and $1 \times 10^{15}\,cm^{-2}$ $He^{2+}$ fluence. Assuming that the variation in the topography-dependent surface potential is negligible, the FWHM should increase with the inhomogeneous defect distribution; the saturated FWHM, together with the smaller CPD upshift, indicates that the occurrence of ion-induced damage is no longer dominant in the dose regime higher than $5 \times 10^{14}\,cm^{-2}$. Crossing over this value, softening of the phonon and the appearance of amorphous carbon can be anticipated. Previously, Buchowicz *et al*. reported that ion irradiation induces structurally amorphorized graphene and significantly reduces mobility while pinning the Fermi level. However, our results demonstrate that tuning of the Fermi level or chemical change is also possible.[29]

To evaluate the chemical change of the surface state induced by the $\alpha$-beam, synchrotron-based high-resolution PES was conducted for the two extreme cases: pristine graphene and graphene treated with an $\alpha$-beam at $1 \times 10^{15}\,cm^{-2}$ ion fluence. First, the valence band measurement was carried out at a photon energy of 72.5 eV; the results are plotted in Fig. 4(a), where the black and red spectra represent the pristine graphene and $He^{2+}$-treated graphene, respectively, and $E_F$ is the zero-binding energy. As the beam energy employed for photoemission in the valence band is higher than that of He I or He II, which are usually used, the synchrotron source

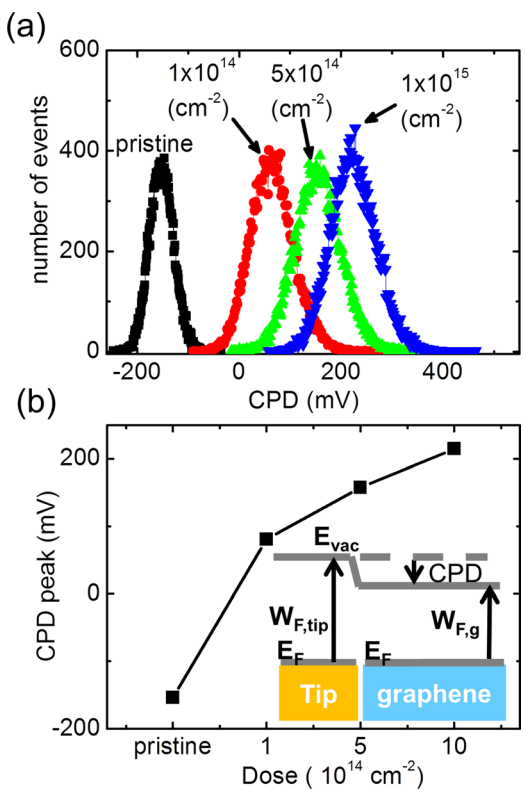


FIG. 3. (a) Distribution of the CPD of Kelvin signals in the various graphene samples. (b) Peak positions of the CPD histograms. The inset shows a schematic of the energy diagram for the tip–graphene system. $E_{vac}$ is the energy level in a vacuum.

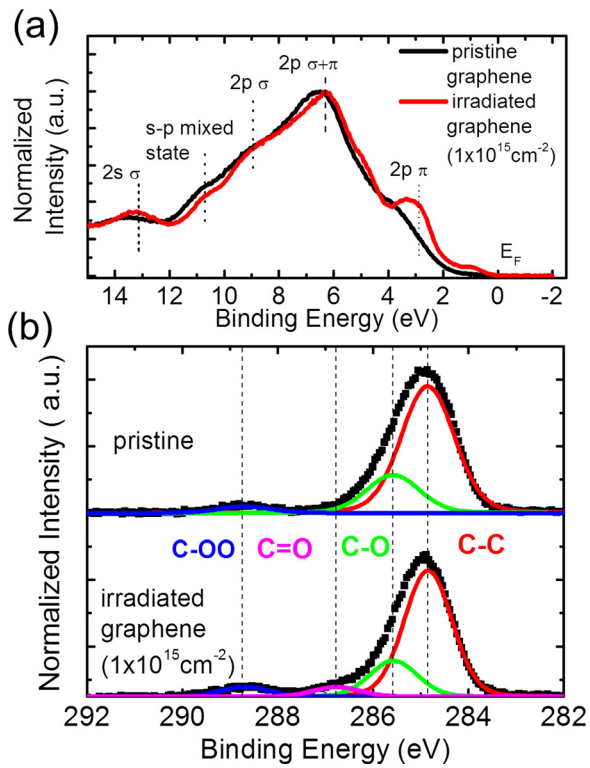


FIG. 4. X-ray photoelectron spectra for (a) valence band and (b) core level for the pristine and irradiated graphene (using $1 \times 10^{15}\,cm^{-2}$). The photon energies used are 72.5 eV for the valence band edge and 650 eV for the core level. The C1s PES signal of the pristine graphene comprised three peaks corresponding to C–C, C–O, and C–OO. C=O is observed only in the irradiated graphene.

would be advantageous in representing variations in the density of states (DOS) while suppressing interference between the initial and final states of the emitted electrons. Also, such high excitation energy can give the valence band DOS over a wider range, stretching to the $C_{2s}$ states. As shown in Fig. 4(a), both samples show a five-band feature, which are assigned to $C_{2p\pi}$ ($0 \sim 4$ eV), the overlap of $C_{2p\pi}$ and $C_{2p\sigma}$ ($\sim$6 eV), $C_{2p\sigma}$ ($\sim$8 eV), the s–p mixed hybridized state ($\sim$11 eV), and $C_{2s}$ ($\sim$8 eV).[30] With $He^{2+}$ treatment, the $C_{2p\pi}$ peak was clearly developed, which is associated with deformation of the carbon network ($sp^2$) or formation of dangling bonds. The whole spectrum was observed to shift towards the Fermi level after the $He^{2+}$-treatment, indicating depletion of electrons, which is consistent with the KPFM results.

Next, we focused on the origin of the doping effect by irradiation using PES about the core levels. Since the graphene is only 0.3 nm thick, surface sensitive methods, such as PES, provide valuable information about the nature of the bonding before and after irradiation. The PES survey scan spectra for the core level were acquired by using a photon energy of 650 eV. In Fig. 4(b), the PES results for C1s of both pristine (top) and $1 \times 10^{15}$ $cm^{-2}$ $He^{2+}$-treated graphene (bottom) are given to identify C/O groups occurring on the surface. Both spectra are referenced to C1s at 284.7 eV and a simple Shirley-type correction is introduced to remove the background noise caused by inelastic electron scattering. Both spectra curves feature asymmetry toward a higher binding energy and relatively broad FWHM of $\sim$2.1 eV due to superposition of the C/O functional groups. To establish the various existing C/O groups, The C1s peaks are divided into four symmetric Gaussian curves at 284.8 eV, 285.6 eV, 287.0 eV, and 288.7 eV, which are assigned to C–C, C–O, C=O, and C–OO, respectively.[31,32] As shown in Fig. 4, the existence of C–O (peak area ratio of 22%) and C–OO (4%) can be confirmed in the C1s for the pristine graphene, but C=O is not detectable before irradiation. However, for the $He^{2+}$-treated graphene, the formation of C=O becomes observable (5%) and the C–OO also increases slightly up to 6%, while C–C is reduced from 74 to 68%. Therefore, it is evident that the carbon bonds broken by the $He^{2+}$ beam are spontaneously reconstructed toward either C=O or C–OO where the formation of an oxygen anion requires hole doping of the graphene, implying that the hole doping effect is closely associated with this bond reconstruction. Consistent with these results, Shin *et al*. demonstrated that highly resistive graphene oxide can be obtained by removing the C=O using a $N_2H_4$ solution and claimed that C=O and C–OO play a major role in hole doping in graphene oxide and that C–N groups compensate for the hole carriers by effectively removing C=O.[33] We attribute the hole doping effect to the charge transfer taking place during bond reconstruction between the irradiation-induced broken C bonds and $O_2$ molecules.[29] The three *ex situ* measurements of KPFM, PES, and Raman spectroscopy were conducted and showed the same doping effect. Exposure to air does not influence the types of doping. Therefore, we supposed this result indicates that the p-doping of graphene induced by $He^{2+}$ irradiation is rather robust. For understanding the more intrinsic transport properties, such as hole or electron conduction, measurement of the conductance–gate voltage plot might be ideal. An intriguing approach is to carry out scanning gate microscopy where the source–drain current can be governed by the bias voltage of the AFM tip.

In conclusion, our results show that $He^{2+}$ irradiation results in the p-doping effect that could be directly determined by KPFM. The effect is attributed to the charge transfer (interaction) between broken C bonds and ambient $O_2$ molecules, which results in C=O or C–OO bonds. Surface-sensitive PES measurements confirm that the C=O and C–OO bond density increases after $He^{2+}$ beam irradiation. Overall, hole doping leads an increase in the work function by as much as 400 mV, where this increase shows a logarithmic behavior with respect to the irradiation dose. The generation of defects using inert gas ions has the advantage of being a simple process with precise tuning of the work function of graphene.

This work was supported by IBS (Institute for Basic Science) and 2012R1A2A1A01009249, and the SRC Centre for Topological Matter (Grant No. 2011-0030787) through the National Research Foundation (NRF), Republic of Korea. The irradiation work and some analyses were supported by the Director, Office of Science, Office of Basic Energy Sciences, and Division of Materials Sciences and Engineering of the U.S. Department of Energy under Contract No. De-Ac02-05Ch11231. Experiments at PLS were supported in part by MSIP and POSTECH.

[1]K. S. Novoselov, A. K. Geim, S. V. Morozov, D. Jiang, M. I. Katsnelson, I. V. Grigorieva, S. V. Dubonos, and A. A. Firsov, Nature **438**(7065), 197–200 (2005).
[2]Y. B. Zhang, Y. W. Tan, H. L. Stormer, and P. Kim, Nature **438**(7065), 201–204 (2005).
[3]S. Ghosh, I. Calizo, D. Teweldebrhan, E. P. Pokatilov, D. L. Nika, A. A. Balandin, W. Bao, F. Miao, and C. N. Lau, Appl. Phys. Lett. **92**(15), 151911 (2008).
[4]K. S. Kim, Y. Zhao, H. Jang, S. Y. Lee, J. M. Kim, K. S. Kim, J. H. Ahn, P. Kim, J. Y. Choi, and B. H. Hong, Nature **457**(7230), 706–710 (2009).
[5]X. S. Li, W. W. Cai, J. H. An, S. Kim, J. Nah, D. X. Yang, R. Piner, A. Velamakanni, I. Jung, E. Tutuc, S. K. Banerjee, L. Colombo, and R. S. Ruoff, Science **324**(5932), 1312–1314 (2009).
[6]C. Jeon, H.-N. Hwang, W.-G. Lee, Y. G. Jung, K. S. Kim, C.-Y. Park, and C.-C. Hwang, Nanoscale **5**, 8210–8214 (2013).
[7]J. S. Choi, J. S. Kim, I. S. Byun, D. H. Lee, M. J. Lee, B. H. Park, C. Lee, D. Yoon, H. Cheong, K. H. Lee, Y. W. Son, J. Y. Park, and M. Salmeron, Science **333**(6042), 607–610 (2011).
[8]D. Teweldebrhan and A. A. Balandin, Appl. Phys. Lett. **94**(1) 013101 (2009).
[9]C. Mattevi, H. Kim, and M. Chhowalla, J. Mater. Chem. **21**(10), 3324–3334 (2011).
[10]Z. Q. Luo, J. Z. Shang, S. H. Lim, D. H. Li, Q. H. Xiong, Z. X. Shen, J. Y. Lin, and T. Yu, Appl. Phys. Lett. **97**(23), 233111 (2010).
[11]S. Chandramohan, J. H. Kang, Y. S. Katharria, N. Han, Y. S. Beak, K. B. Ko, J. B. Park, H. K. Kim, E. K. Suh, and C. H. Hong, Appl. Phys. Lett. **100**(2), 023502 (2012).
[12]K. K. Kim, A. Reina, Y. M. Shi, H. Park, L. J. Li, Y. H. Lee, and J. Kong, Nanotechnology **21**(28), 285205 (2010).
[13]S. Kwon, E. S. Lee, H. Seo, K. J. Jeon, C. C. Hwang, Y. H. Kim, and J. Y. Park, Surf. Sci. **612**, 37–41 (2013).
[14]S. Kwon, J. H. Ko, K. J. Jeon, Y. H. Kim, and J. Y. Park, Nano Lett. **12**(12), 6043–6048 (2012).
[15]H. G. Jee, K. H. Jin, J. H. Han, H. N. Hwang, S. H. Jhi, Y. D. Kim, and C. C. Hwang, Phys. Rev. B **84**(7), 075457 (2011).
[16]S. Nakaharai, T. Iijima, S. Ogawa, S. Suzuki, S.-L. Li, K. Tsukagoshi, S. Sato, and N. Yokoyama, ACS Nano **7**(7), 5694–5700 (2013).

[17]S. Kwon, S. Choi, H. J. Chung, H. Yang, S. Seo, S. H. Jhi, and J. Y. Park, Appl. Phys. Lett. **99**(1), 013110 (2011).
[18]S. Kwon, H. J. Chung, S. Seo, and J. Y. Park, Surf. Interface Anal. **44**(6), 768–771 (2012).
[19]O. Lehtinen, J. Kotakoski, A. V. Krasheninnikov, A. Tolvanen, K. Nordlund, and J. Keinonen, Phys. Rev. B **81**(15), 153401 (2010).
[20]L. G. Cançado, K. Takai, T. Enoki, M. Endo, Y. A. Kim, H. Mizusaki, A. Jorio, L. N. Coelho, R. Magalhães-Paniago, and M. A. Pimenta, Appl. Phys. Lett. **88**(16), 163106 (2006).
[21]L. G. Cancado, A. Jorio, E. H. M. Ferreira, F. Stavale, C. A. Achete, R. B. Capaz, M. V. O. Moutinho, A. Lombardo, T. S. Kulmala, and A. C. Ferrari, Nano Lett. **11**(8), 3190–3196 (2011).
[22]S. Pisana, M. Lazzeri, C. Casiraghi, K. S. Novoselov, A. K. Geim, A. C. Ferrari, and F. Mauri, Nature Mater. **6**(3), 198–201 (2007).
[23]J. Yan, Y. B. Zhang, P. Kim, and A. Pinczuk, Phys. Rev. Lett. **98**(16), 166802 (2007).
[24]A. Das, S. Pisana, B. Chakraborty, S. Piscanec, S. K. Saha, U. V. Waghmare, K. S. Novoselov, H. R. Krishnamurthy, A. K. Geim, A. C. Ferrari, and A. K. Sood, Nat. Nanotechnol. **3**(4), 210–215 (2008).
[25]C. Casiraghi, S. Pisana, K. S. Novoselov, A. K. Geim, and A. C. Ferrari, Appl. Phys. Lett. **91**(23), 233108 (2007).
[26]M. Nonnenmacher, M. P. Oboyle, and H. K. Wickramasinghe, Appl. Phys. Lett. **58**(25), 2921–2923 (1991).
[27]S. Ryu, L. Liu, S. Berciaud, Y. J. Yu, H. T. Liu, P. Kim, G. W. Flynn, and L. E. Brus, Nano Lett. **10**(12), 4944–4951 (2010).
[28]Y. J. Yu, Y. Zhao, S. Ryu, L. E. Brus, K. S. Kim, and P. Kim, Nano Lett. **9**(10), 3430–3434 (2009).
[29]G. Buchowicz, P. R. Stone, J. T. Robinson, C. D. Cress, J. W. Beeman, and O. D. Dubon, Appl. Phys. Lett. **98**(3), 032102 (2011).
[30]A. Bianconi, S. B. M. Hagstrom, and R. Z. Bachrach, Phys. Rev. B **16**(12), 5543–5548 (1977).
[31]D. Yang, A. Velamakanni, G. Bozoklu, S. Park, M. Stoller, R. D. Piner, S. Stankovich, I. Jung, D. A. Field, C. A. Ventrice, and R. S. Ruoff, Carbon **47**(1), 145–152 (2009).
[32]D. R. Dreyer, S. Park, C. W. Bielawski, and R. S. Ruoff, Chem. Soc. Rev. **39**(1), 228–240 (2010).
[33]H. J. Shin, K. K. Kim, A. Benayad, S. M. Yoon, H. K. Park, I. S. Jung, M. H. Jin, H. K. Jeong, J. M. Kim, J. Y. Choi, and Y. H. Lee, Adv. Funct. Mater. **19**(12), 1987–1992 (2009).